arXiv:1203.4479v2 [astro-ph.CO] 2 May 2012

# Local and non-local measures of acceleration in cosmology

Philip Bull[1, *] and Timothy Clifton[1, 2, †]
[1]*Department of Astrophysics, University of Oxford, UK.*
[2]*School of Physics and Astronomy, Queen Mary University of London, UK.*

Current cosmological observations, when interpreted within the framework of a homogeneous and isotropic Friedmann-Lemaître-Robertson-Walker (FLRW) model, strongly suggest that the Universe is entering a period of accelerating expansion. This is often taken to mean that the expansion of space itself is accelerating. In a general spacetime, however, this is not necessarily true. We attempt to clarify this point by considering a handful of local and non-local measures of acceleration in a variety of inhomogeneous cosmological models. Each of the chosen measures corresponds to a theoretical or observational procedure that has previously been used to study acceleration in cosmology, and all measures reduce to the same quantity in the limit of exact spatial homogeneity and isotropy. In statistically homogeneous and isotropic spacetimes, we find that the acceleration inferred from observations of the distance-redshift relation is closely related to the acceleration of the spatially averaged universe, but does not necessarily bear any resemblance to the average of the local acceleration of spacetime itself. For inhomogeneous spacetimes that do not display statistical homogeneity and isotropy, however, we find little correlation between acceleration inferred from observations and the acceleration of the averaged spacetime. This shows that observations made in an inhomogeneous universe can imply acceleration without the existence of dark energy.

PACS numbers: 98.80.Jk

## I. INTRODUCTION

The question of if, and why, the expansion of the Universe is accelerating is one of the foremost problems in fundamental physics today. Observations of distant Type Ia supernovae are well-fit by homogeneous and isotropic Friedmann-Lemaître-Robertson-Walker (FLRW) solutions of general relativity, but only if a substantial fraction of the energy density in the Universe is in the form of a cosmological constant. For this constant to take the value required by observations, however, requires an extraordinary degree of fine-tuning. Many authors have attempted to remedy this situation by proposing modifications to gravity, the existence of negative-pressure components of the cosmological fluid, new scalar fields, and a host of other exotic mechanisms. Others have sought to explain it by modifying the basic assumptions of cosmology itself, such as the Cosmological Principle.

Our aim here is to clarify what is meant by acceleration in an inhomogeneous universe, and to study how different types of acceleration can arise within the context of relativistic cosmology. We do not consider the existence of any strange new matter fields or modifications to Einstein's equations, but we do allow for the Universe to be strongly inhomogeneous below a certain scale. It is found that observations made over large distances (e.g. using supernova and CMB observations) are best modeled using non-local averages of geometric quantities. The acceleration that one can infer from these large-scale probes of cosmology is not necessarily similar to any locally defined measures of acceleration, and does not necessarily imply that the expansion of space itself is accelerating at any point.

Following Hirata & Seljak [1] and Clarkson & Umeh [2], we consider multiple different measures of acceleration:

(a). The local acceleration of nearby observers in a small volume of space, as governed by the Raychaudhuri equation;

(b). The acceleration inferred by fitting an FLRW distance-redshift relation to Hubble diagrams constructed from observations made over large distances;

(c). The acceleration inferred by constructing a Hubble diagram from local observations (i.e. at $z \simeq 0$), as described by Kristian and Sachs [3];

(d). The average acceleration of a large volume of space, as calculated using Buchert's scalar averaging procedure [4].

For an exactly homogeneous and isotropic FLRW model, all of these measures are identical. In the general case, however, they can be quite different, to the point that some of them can show strong acceleration, while others show deceleration.

Measures (a) and (c) are purely local, and depend only on the curvature of spacetime within the neighbourhood of a point (in the limit of geometric optics). Measures (b) and (d), however, are both inherently non-local in nature. Measure (a) describes the actual, dynamical acceleration of a volume of space, while measure (b) corresponds to what is measured in, for example, supernova surveys. Measure (c) is a local measure of acceleration,

---

[*] Electronic address: Phil.Bull@astro.ox.ac.uk
[†] Electronic address: Tim.Clifton@astro.ox.ac.uk

based on inferences made using the luminosity distance-redshift relation within a very small region of spacetime. Measure (d) corresponds to the theoretical procedure of fitting a smooth effective model to the real, inhomogeneous Universe (the question of how best to do this is still very much an open one, but the simplest and best-known procedure is the scalar averaging formalism developed by Buchert [5, 6]). We will discuss all of these measures in detail in what follows.

Constructing relativistic models of the real, inhomogeneous Universe is difficult, but a number of attempts have met partial success in addressing the problem. Realistic density fields can be described using perturbations to exact FLRW solutions. However, at least to quadratic order in perturbations, the effect of inhomogeneities on the overall behaviour of the spacetime often turns out to be small, with the average evolution and optical properties of the model remaining close to the unperturbed background values [1, 7–17]. There have been suggestions that effects at higher orders in perturbations could be important [2, 12], and recent studies of non-linear collapse which make use of a gradient expansion also find potentially significant effects [18, 19]. These claims require further analysis if they are to be confirmed, however. The main drawback of the perturbative approach is that the solutions obtained are not exact, and so it is unclear if we are neglecting or incorrectly estimating aspects of the fully-relativistic behaviour of the spacetime.

An alternative approach involves studying exact, inhomogeneous solutions to Einstein's equations. As the geometry of spacetime is known from the outset, the non-linear evolution of space, and light rays within it, can be calculated in a fully rigorous manner, without recourse to perturbative analyses. This approach tends to require a high degree of symmetry, however, placing strong restrictions on what it is possible to model [20]. For example, backreaction effects in Swiss Cheese models (constructed by joining together spherically-symmetric inhomogeneous regions with a FLRW solution) are known to be small [21]. This is confirmed by ray tracing studies through a variety of similar exact solutions [21–28]. Additionally, inhomogeneous models with general fluid content are difficult to work with [29–31], and so most modeling attempts make do with a dust-only stress-energy tensor. This is itself problematic, as high-density regions tend to rapidly collapse in inhomogeneous pressureless fluids, forming singularities and resulting in unrealistic, pathological behaviour.

Finally, more heuristic analyses have been attempted [21, 32–38]. These often employ disjoint regions of different exact solutions. The dynamical evolution within each region is therefore well defined, but the ensemble as a whole does not satisfy Einstein's equations at the boundaries between regions. This approach relaxes the restrictive symmetry requirements that are necessary when using exact solutions, but introduces its own ambiguities. Indeed, the chosen boundary conditions can sometimes dominate the behaviour of the model [33], and it is not clear whether the resulting spacetime approximates any actual solution of Einstein's equations or not.

In this paper we consider the latter two of these approaches, as the situation of small perturbations around an exact FLRW geometry is well-studied already [9, 16, 39–42]. The format of the paper is as follows. In Section II, we discuss in detail the different measures of acceleration summarised above, and how they can be calculated in a general spacetime. The conditions for these measures to show acceleration, and their relation to observable quantities (if any), is discussed. Section III sets out three different inhomogeneous models: the spherical collapse model, constructed from disjoint FLRW regions; the Kasner-EdS model, an exact solution with alternating expanding vacuum and collapsing dust regions along a line of sight [43–47]; and the Lemaître-Tolman-Bondi model, an exact, spherically-symmetric dust solution [48–50]. The volume of space in all of these models is locally decelerating everywhere, and yet we find that observations made within them can still exhibit acceleration.

In Sections IV, V, and VI, we present our results for each of the models. We find that the acceleration inferred by observers from the Hubble diagram, constructed over large distances, is most closely correlated with the dynamical behaviour of the *averaged* spacetime, and not with its local acceleration. The local acceleration, however, is well modeled by Hubble diagrams that are constructed locally, using the Kristian-Sachs formalism. This result suggests that we should use non-local averages of the geometry to interpret observations made over large distances, and local geometry to interpret observations made locally. Interpreting observations within the wrong framework can lead to incorrect inferences about what is causing the acceleration. This appears to us to provide some insight into the question of whether the apparent acceleration we observe is necessarily caused by the presence of a non-zero cosmological constant, or whether it could be caused by some backreaction effect within the inhomogeneous spacetime. Finally, in Section VII we discuss our results in the context of previous claims involving backreaction and the nature of the apparent acceleration of the Universe.

## II. MEASURES OF ACCELERATION

In this section we discuss the four measures of acceleration that were listed in Section I. Each measure has associated with it a *deceleration parameter*. For each definition, we set out its theoretical basis and physical interpretation, list the conditions necessary for acceleration to occur, and describe the relation of the deceleration parameter associated with this measure to observable quantities. The measures are summarised in Table I, at the end of the section.

### (a) Local volume acceleration

A congruence of time-like geodesics, $u^a$, describing the world-lines of a set of observers comoving within a cosmological fluid can be decomposed such that [51]

$$u_{a;b} = \frac{1}{3}\Theta h_{ab} + \sigma_{ab} + \omega_{ab}, \tag{1}$$

where subscript ; denotes a covariant derivative, and $h_{ab} = g_{ab} + u_a u_b$ is the projection tensor. The kinematic quantities in this equation are the expansion scalar, $\Theta$, the shear, $\sigma_{ab}$, and the vorticity, $\omega_{ab}$, which correspond to the trace, symmetric trace-free, and antisymmetric parts of $u_{a;b}$, respectively. This decomposition is a fully covariant procedure, valid for any spacetime.

For irrotational flows ($\omega_{ab} = 0$), the fluid flow becomes hypersurface orthogonal, with the projection tensor becoming the induced metric of the orthogonal 3-spaces. The field equations then give (with $8\pi G = 1$)

$$\dot{\Theta} = -\frac{1}{3}\Theta^2 - \frac{1}{2}(\rho + 3p) + \Lambda - 2\sigma^2, \tag{2}$$

where the over-dot denotes a derivative with respect to proper time along $u^a$, and where $\sigma^2 = \frac{1}{2}\sigma_{ab}\sigma^{ab}$, and $\rho$, $p$ and $\Lambda$ are the energy density, pressure and cosmological constant, respectively. The Gauss embedding equation for these hypersurfaces is

$$\frac{1}{3}\Theta^2 = \rho + \Lambda + \sigma^2 - \frac{1}{2}{}^{(3)}\mathcal{R}, \tag{3}$$

where ${}^{(3)}\mathcal{R}$ is the Ricci scalar constructed from $h_{ab}$.

By analogy with the deceleration parameter in an FLRW spacetime, one can then define a local volume deceleration parameter,

$$q_\Theta = -1 - 3\frac{\dot{\Theta}}{\Theta^2} = \frac{3}{\Theta^2}\left[\frac{1}{2}(\rho + 3p) - \Lambda + 2\sigma^2\right], \tag{4}$$

corresponding to the monopole of the deceleration of the expansion rate of a set of neighbouring particles following $u^a$. This measure is said to be accelerating when $q_\Theta < 0$, which from Eq. (4) can be seen to occur if and only if $p < -\frac{1}{3}\rho$ or $\Lambda > 0$.

Now, $q_\Theta$ is a local measure of acceleration, defined only in the neighbourhood of a point in spacetime. Determining $q_\Theta$ from observations therefore requires $\Theta$ (and its first derivative) to be determined using observations within the neighbourhood of a single point in spacetime only. These observations need to be of the rate of change of proper distance between particles in their own rest-frame, which is not necessarily the same as the angular diameter distance or luminosity distance (for these see measure (c), below). The Universe is extremely inhomogeneous on small scales, and so this measure of acceleration is likely to display considerable spatial variation. A local measurement of $q_\Theta$ need not, then, be representative of the mean local volume acceleration.

### (b) Observed acceleration (as inferred from the Hubble diagram)

To date, the strongest observational evidence for an accelerating universe comes from the distance-redshift relation, which is measured using "standardisable candles" (such as Type Ia supernovae), as well as the CMB. By fitting this data to the relations derived from the FLRW solutions of Einstein's equations, one finds that models with $\Omega_\Lambda > 0$ are strongly favoured, while those with $\Omega_\Lambda = 0$ are ruled out to a high degree of confidence. Under the assumption that spacetime is well-described by FLRW, this constitutes strong evidence for accelerating expansion.

A key step in this procedure is the fitting of the FLRW distance-redshift relation to data. Performing a series expansion in the angular diameter distance about $z = 0$ gives

$$d_A(z) = \frac{cz}{H_0}\left(1 - \frac{1}{2}(3 + q_0)z + \mathcal{O}(z^2)\right), \tag{5}$$

where $H_0$ is the inferred Hubble rate at $z = 0$, and $q_0$ is the inferred deceleration parameter. The value of $q_0$ can be found in a purely observational manner by taking derivatives of the fitted distance-redshift relation [52],

$$q_0 = -\left.\frac{d''_A}{d'_A}\right|_0 - 3, \tag{6}$$

where primes denote derivatives with respect to redshift, and where subscript 0 denotes that a quantity is evaluated at the observer. Note that this measure of deceleration is inferred from observations over large distances, and so assigns information to a point in spacetime based on information obtained from the entire extended region over which observations have been made. This is a highly non-local process.

Eq. (6) is derived from the distance-redshift relation in FLRW geometry, but one should note that the existence of such a geometry is not required in order to infer $q_0$ from observations. What we are doing here should instead be considered simply as a fitting procedure. Eq. (6) is then an observable in *any* spacetime (after averaging over the celestial sphere), and so anyone can measure $q_0$ if they are willing to interpret their observations within the framework of an FLRW model. We call the acceleration inferred by this fitting of FLRW relations to the monopole of the distance-redshift relation the *observed acceleration.*

The distance-redshift relation can be calculated in a general spacetime by solving the Sachs optical equations for bundles of null geodesics. With vanishing vorticity, these are

$$\begin{aligned} \frac{d\theta}{d\lambda} + \theta^2 + |\hat{\sigma}|^2 &= -\frac{1}{2}R_{ab}k^a k^b & (7)\\ \frac{d\hat{\sigma}}{d\lambda} + 2\theta\hat{\sigma} &= C_{abcd}(t^*)^a k^b (t^*)^c k^d, & (8) \end{aligned}$$

where $\lambda$ is an affine parameter along the bundle, $R_{ab}$ and $C_{abcd}$ are the Ricci and Weyl tensors of the spacetime, $\theta$ and $\hat{\sigma}$ are the expansion and (complex) shear scalars of the null geodesics, $k^a$ is a tangent vector to the null curves, and $t^a$ are (complex) vectors spanning a two-dimensional screen space orthogonal to $k^a$. The expansion scalar is related to the angular diameter distance measured along the bundle by $\theta = d(\ln(d_A))/d\lambda$. Substituting this into Eq. (7) yields

$$\frac{d^2(d_A)}{d\lambda^2} = -d_A \left( |\hat{\sigma}|^2 + \frac{1}{2} R_{ab} k^a k^b \right). \tag{9}$$

The luminosity distance is related to the angular diameter distance by the reciprocity theorem [53], which gives $d_L = (1+z)^2 d_A$.

The affine distance-redshift relation for a general spacetime is given by [54]

$$\frac{dz}{d\lambda} = -(1+z)^2 H_{||}(z), \tag{10}$$

where $H_{||} = \frac{1}{3}\Theta + \sigma_{ab} e^a e^b$ is the expansion rate along the line of sight, $e^a$. Equations (8)–(10) can be solved to give the angular diameter distance-redshift relation, $d_A(z)$, in any given direction, at any given point in spacetime. This procedure can be repeated for every direction on the sky, and an FLRW model can be fitted to the monopole of the resulting angular distribution. The best-fit model can then be used to find $q_0$. We denote the result of this procedure in a general spacetime as $q_{\rm obs}$.

We consider this definition of acceleration to correspond most closely to the one used by observers. It is a non-local measure, since it depends on solutions to the Sachs equations, which describe bundles of null geodesic curves that extend through the spacetime. In effect, the measurement of $q_{\rm obs}$ depends on finding the entire past null cone of an observer out to some $z$, and fitting some distance-redshift relation to it. The conditions for a spacetime to have $q_{\rm obs} < 0$ are therefore complicated, in general. As we will see below, it is possible to find spacetimes that are quite different from simple $\Lambda$-dominated FLRW models that nevertheless have $q_{\rm obs} < 0$.

### (c) Acceleration from local observations (using the Kristian-Sachs formalism)

The measure of acceleration we just described has the disadvantage of requiring solutions to the Sachs equations to be found, as a function of redshift and angle on the observer's sky. This can be a difficult task in general, as it requires detailed knowledge of the geometry of spacetime. Instead, one can use the Kristian-Sachs formalism [3] to obtain a fully general and covariant series expansion of the distance-redshift relation about an observer without needing to consider solutions to the geodesic equations at all. Furthermore, the expansion can be decomposed directly into covariant spherical harmonics about the observer, allowing the monopole term to be calculated straight away [2].

This procedure has been spelled out in detail by Clarkson and Umeh [2]. The generalised form of Eq. (5) is

$$d_A = \frac{z}{[K^a K^b \nabla_a u_b]_0} \left( 1 - \left[ \frac{K^a K^b K^c \nabla_a \nabla_b u_c}{2(K^d K^e \nabla_d u_e)^2} \right]_0 z + \mathcal{O}(z^2) \right), \tag{11}$$

where the past-pointing null direction can be written in terms of the tangent vector to a comoving observer's world-line, $u^a$, and a direction on their sky, $e^a$, as

$$K^a = \frac{k^a}{[u_b k^b]_0} = -u^a + e^a. \tag{12}$$

The subscript 0 again denotes evaluation at the observer's location. The terms in Eq. (11) can be expanded using a covariant decomposition in spherical harmonics. In order to facilitate this expansion, it is useful to invert Eq. (11) to give

$$z = [K^a K^b \nabla_a u_b]_0 d_A + \frac{1}{2}[K^a K^b K^c \nabla_a \nabla_b u_c]_0 d_A^2 + \mathcal{O}(d_A^3). \tag{13}$$

All of the terms that we wish to expand are now in the numerator. Comparing the monopoles of the coefficients in Eq. (13) with the corresponding FLRW relation (with $8\pi G = 1$) then gives

$$q_{\rm KS} = \frac{3}{\Theta^2} \left[ \frac{1}{2}(\rho + 3p) - \Lambda + 6\sigma^2 \right]_0, \tag{14}$$

where we have used $H_0 = \frac{1}{3}\Theta$, which corresponds to the monopole of this term, rather than its full spherical harmonic expansion. This corresponds most closely with the way that $H_0$ is typically used in observational studies; the monopole of $H_0$ tends to be determined separately from other quantities. From Eq. (14), it can be seen that $q_{\rm KS} \geq 0$ unless $p < -\frac{1}{3}\rho$ or $\Lambda > 0$. That is, acceleration of this measure can only occur if there is a cosmological constant, or if an exotic fluid with negative pressure is present.

There is clearly some similarity between the deceleration parameter of the local volume, $q_\Theta$, and that which is obtained from the local distance-redshift relation, $q_{\rm KS}$. Both measures of acceleration are local (depending only on quantities defined within the neighbourhood of the observer), and both are given by expressions that differ only by a term involving the shear scalar. This does not, however, mean that these two measures of acceleration are the same. They correspond to different physical quantities.

The relation between the Kristian-Sachs and observational acceleration measures is less clear. This has to do with the non-locality of the latter; if the Hubble diagram could be measured precisely at $z = 0$ (i.e. in the limit of geodesics of zero affine length), we would find $q_{\rm obs} = q_{\rm KS}$. But, because real observations necessarily cover a range of redshifts, the process of fitting a curve to the data and extrapolating that back to $z = 0$ means that in general we will have $q_{\rm obs} \neq q_{\rm KS}$. This phenomenon has been investigated using real data in [55]. As we shall see in what follows, even the signs of $q_{\rm obs}$ and $q_{\rm KS}$ can be different. That is, a locally-decelerating spacetime can still have a Hubble diagram that implies acceleration.

### (d) Acceleration of the average (using Buchert's formalism)

One method of constructing a homogeneous and isotropic 'effective' model within which observations can be interpreted involves taking averages of geometrical quantities over space-like hypersurfaces. The hope is then that the behaviour of the averaged model will capture some aspects of the real spacetime, both in terms of its dynamics, and the observational quantities that are calculated within it. Many such averaging procedures exist [56], but here we will concentrate on the Buchert scalar averaging formalism [4]. This is the most widely used formalism in the literature.

Buchert's method proceeds as follows. First of all, the spacetime is filled with a congruence of (irrotational) curves. It is then foliated with a set of space-like hypersurfaces orthogonal to these curves. The proper 3-volume of a domain, $\mathcal{D}$, on a given hypersurfaces is

$$V_{\mathcal{D}} = \int_{\mathcal{D}} \sqrt{-h}\; d^3x, \tag{15}$$

where $h_{ij}$ is the induced metric on the hypersurface, and $h = \det\, h_{ij}$. In general, the induced metric will be a function of time, and so the volume is time-dependent as well. The proper volume-weighted average of a scalar quantity, $S$, over a spatial domain, $\mathcal{D}$, can then be written as

$$\langle S \rangle = V_{\mathcal{D}}^{-1} \int_{\mathcal{D}} S(\vec{x}, t) \sqrt{-h}\; d^3x. \tag{16}$$

Spatial averaging and time evolution do not, in general, commute. They instead obey the commutation relation

$$\partial_t \langle S \rangle - \langle \partial_t S \rangle = \langle \Theta S \rangle - \langle \Theta \rangle \langle S \rangle. \tag{17}$$

An 'effective' homogeneous model can be constructed by averaging over domain sizes greater than the statistical homogeneity scale of the underlying inhomogeneous spacetime. An effective scale factor for the resulting model can then be defined as

$$a_{\mathcal{D}}(t) = \left( \frac{V_{\mathcal{D}}(t)}{V_{\mathcal{D}}(t_0)} \right)^{\frac{1}{3}}, \tag{18}$$

where $t_0$ is some fiducial time. For geodesic curves, and pressure-free matter, we can use this formalism to construct analogues to the Friedmann and Raychaudhuri equations,

$$\begin{aligned} 3H_{\mathcal{D}}^2 &= 8\pi G \langle \rho \rangle + \Lambda - \frac{1}{2}\left( Q_{\mathcal{D}} + \langle {}^{(3)}\mathcal{R} \rangle \right) \\ 3\frac{\ddot{a}_{\mathcal{D}}}{a_{\mathcal{D}}} &= -8\pi G \langle \rho \rangle + \Lambda + Q_{\mathcal{D}}, \end{aligned} \tag{19}$$

where $H_{\mathcal{D}} = \dot{a}_{\mathcal{D}}/a_{\mathcal{D}}$. Over-dots denote partial differentiation with respect to $t$, the proper time along curves orthogonal to the 3-space. The *kinematical backreaction scalar* is defined to be

$$Q_{\mathcal{D}} = \frac{2}{3}\left( \langle \Theta^2 \rangle - \langle \Theta \rangle^2 \right) - 2\langle \sigma^2 \rangle. \tag{20}$$

A deceleration parameter for the averaged hypersurfaces can then be defined, by analogy with FLRW cosmological models, as

$$q_{\mathcal{D}} = -\frac{1}{H_{\mathcal{D}}^2} \frac{\ddot{a}_{\mathcal{D}}}{a_{\mathcal{D}}}. \tag{21}$$

An effective distance-redshift relation can also be found for the averaged model by assuming that light rays follow null geodesics of the averaged spacetime, and that geodesic observers are comoving in the average geometry.

In general, the deceleration parameter $q_{\mathcal{D}}$ is non-local, and not directly observable, as it depends on averages over extended space-like hypersurfaces. From Eq. (19), one can see that if the averaged spatial Ricci curvature, $\langle {}^{(3)}\mathcal{R} \rangle$, and backreaction, $Q_{\mathcal{D}}$, behave in a certain way, then it is possible to have $q_{\mathcal{D}} < 0$ without having $\Lambda > 0$ or $\langle \rho \rangle < 0$. In particular, spacetimes consisting of collapsing regions in an expanding background can exhibit this behaviour, which has led some to claim that the apparent cosmic acceleration inferred from supernova observations could instead be explained as a consequence of the variance of the inhomogeneous expansion rate that enters into the definition of $Q_{\mathcal{D}}$ [5, 6, 36, 39, 57, 58]. We will examine this claim in detail later on, but for now will just note that it is possible for the Buchert averaged model to accelerate, even if $q_{\Theta} > 0$ everywhere.

| **Measure** | **Local** | **Support** | **Observable** |
|---|---|---|---|
| Local volume, $q_{\Theta}$ | Yes | Spacetime point | In principle |
| Observational, $q_{\rm obs}$ | No | Null geodesic | Yes |
| Kristian-Sachs, $q_{\rm KS}$ | Yes | Spacetime point | In principle |
| Buchert average, $q_{\mathcal{D}}$ | No | Spatial domain | No |

Table I: Summary of the different measures of acceleration defined in Section II.

Quantities of particular interest are the deceleration parameters that observers in a given region of spacetime should *expect* to infer, rather than the actual values of these parameters at single points (which may not be representative). To this end, we also use Eq. (16) to average our various measures of acceleration. For example, $\langle q_{\rm KS} \rangle$ will be taken to correspond to the value of the

Kristian-Sachs deceleration parameter that a typical observer would expect to measure in a given region. Unless specified otherwise, the averaging domain is taken to be larger than the homogeneity scale of the model[1].

## III. INHOMOGENEOUS COSMOLOGICAL MODELS

We now consider a number of different relativistic models, and how the measures of acceleration defined in Section II can be calculated in each of them. We will primarily be interested in cases with vanishing cosmological constant, as a non-zero $\Lambda$ generically results in accelerating expansion in all of the measures discussed above. The models we consider are chosen as illustrative examples, as they are capable of showing acceleration in some measures, while displaying deceleration in others.

### A. Spherical collapse model

In this section we consider the spherical collapse model, which consists of an ensemble of disjoint FLRW regions [59–62]. It is not an exact solution to Einstein's equations (distinct FLRW models cannot satisfy the appropriate junction conditions on their shared boundary), but provides a useful toy model of collapsing structures in an otherwise expanding universe. By virtue of each individual region being homogeneous, spatial averages take a particularly simple form in spherical collapse models. A scalar quantity $S$ may be averaged simply by taking the sum of its values in the different regions weighted by the proper 3-volume of each region, $V$, at a given time [7, 34],

$$\langle S\rangle = \frac{\sum_i S_i V_i}{\sum_i V_i}. \tag{22}$$

We wish to model the collapse of structures in an expanding background, as this configuration is known to lead to acceleration of the Buchert averaged spacetime, $q_{\mathcal{D}} < 0$ [7, 34]. To this end, we select alternating regions of collapsing, spatially closed and dust-dominated regions, and expanding, spatially open vacuum regions, as illustrated in Fig. 1. We model the regions using FLRW geometry (with $\Lambda = 0$), and refer to them as Regions I and II, respectively. The collapsing regions are chosen so that they have a comoving size of order 10% of the vacuum regions at the present time. As we look further back in time, the collapsing regions increasingly dominate the proper spatial volume.

In what follows we will use the following form for the FLRW metric,

$$ds^2 = dt^2 - \frac{a^2\left(dX^2+dY^2+dZ^2\right)}{[1+\frac{k}{4}(X^2+Y^2+Z^2)]^2}, \tag{23}$$

and take the individual domains to have depth $X_{\mathcal{D}}$. The proper volume of each domain is

$$V_i = \int_{\mathcal{D}_i} \frac{a_i^3 dX dY dZ}{[1+(k_i/4)(X^2+Y^2+Z^2)]^3}, \tag{24}$$

and the comoving depth of a domain is

$$\chi_i = \int_0^{X_{\mathcal{D}_i}} \frac{dX}{1+(k_i/4)(X^2+Y^2+Z^2)}. \tag{25}$$

The effective scale factor, defined in Eq. (18), is

$$a_{\mathcal{D}}(t) = \left(\frac{\sum_i V_i(t)}{\sum_i V_i(t_0)}\right)^{\frac{1}{3}}, \tag{26}$$

and the Buchert average deceleration parameter $q_{\mathcal{D}}$ is calculated according to Eq. (21).

The distance-redshift relation is required to find $q_{\rm obs}$. It can be found by solving the Sachs optical equations for a ray passing through a number of different FLRW regions. All that is required is to ensure continuity of the affine parameter, $\lambda$, the redshift, $z$, the angular diameter distance, $d_A$, and the expansion scalar, $\theta$, at the boundary, as a ray leaves one region and enters another. These conditions impose no restrictions on the individual FLRW regions. Their size, matter content, and expansion rate can be chosen separately. We choose the cosmic time in individual regions such that it is continuous on the boundary between them.

The Sachs equations in each region are given by

$$\frac{d^2(d_A)}{d\lambda^2} = -4\pi G\rho_i\ (1+z)^2 d_A, \tag{27}$$

with 4-vector tangent to the null curves given by

$$k^a = \left(1+z, \pm\frac{1+z}{a_i}\sqrt{1+\frac{1}{4}k_i X^2}, 0, 0\right). \tag{28}$$

The redshift as a function of affine distance is then

$$\frac{dz}{d\lambda} = -H_i(1+z)^2. \tag{29}$$

We have not used $1+z = a^{-1}$, as the total redshift along a ray, $z(\lambda)$, is not the same as the redshift that one would obtain by ray-tracing through a single FLRW region.

We propagate the light rays through each region in turn, until the edge of the region is reached at some coordinate distance $X_i$ (which we call the 'length' of the

---

[1] It should be noted that this averaging scheme is weighted by proper volume, and so the density of observers is implicitly assumed to be weighted in a similar manner. Of course, this need not be the case, and other ways of distributing observers throughout space could be considered. This would affect what a 'typical' observer should expect to see. We do not consider this question further here.

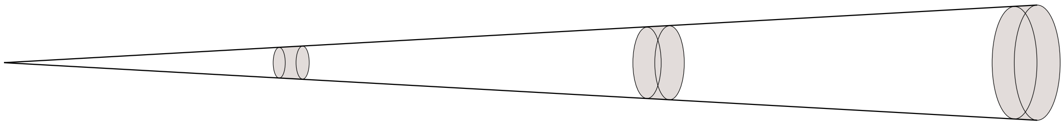

Figure 1: Schematic representation of a line-of-sight through a universe with alternating expanding vacuum regions (clear), and collapsing dust regions (grey).

region). This length is a function of time (evaluated at the instant the ray enters a region), chosen so that the ray travels a proper distance in each region proportional to the fraction of the proper volume taken up by that region on a surface of constant $t$, i.e.

$$\frac{a_I \chi_I}{a_{II} \chi_{II}} = \frac{V_I}{V_{II}}. \tag{30}$$

This choice takes into account not only the different expansion rates of the two different regions along the line of sight, but also the fact that as we go forwards in time the number density of dust regions should be expected to decrease. For simplicity, we fix the (comoving) length of the collapsing region, $\chi_I$, and then solve Eq. (30) for $\chi_{II}$ on entering each new region.

The redshift through the model is given by integrating Eq. (29). There is a blueshift as the photons pass through collapsing regions, and a redshift as they pass through expanding regions. The distance increases despite the blueshift, and the distance-redshift relation becomes multi-valued. This leads to it taking on a jagged appearance, although the distance remains smooth as a function of affine parameter. The observational deceleration parameter can be calculated by fitting an FLRW model with dust, curvature, and $\Lambda$ to the jagged distance-redshift curve, using a simple least-squares procedure. The FLRW deceleration parameter, defined by Eq. (6), can then be calculated to give $q_{\rm obs}$.

The local volume deceleration parameter in each FLRW region is given by Eq. (4). In our chosen spherical collapse model, $\Omega_\Lambda = 0$ in both regions, and $\Omega_m = 0$ in the vacuum region, so the average of the local deceleration parameter reduces to

$$\langle q_\Theta \rangle = \frac{1}{2} \frac{\Omega_{m,I} V_I}{V_I + V_{II}} \bigg|_0 , \tag{31}$$

which is positive definite (i.e. decelerating everywhere). The equality $q_\Theta = q_{\rm KS}$ holds, since each region is FLRW, and therefore has vanishing shear.

### B. Kasner-EdS model

In the previous section we considered the spherical collapse model, which consists of disjoint regions of different FLRW spacetimes. This model is simple to work with, but only forms an approximate solution of Einstein's equations. In this section we consider an exact solution that is inhomogeneous along the line of sight, with alternating regions of collapsing dust and expanding vacuum, as illustrated in Figure 1. We take the two space-like directions orthogonal to the line of sight to span a plane symmetric subspace, and enforce statistical homogeneity along the line of sight only.

In order to prevent the rapid formation of singularities that often occurs when dust is allowed to collapse in general relativistic models, we will take the dust dominated regions to be locally spatially homogeneous and isotropic. These symmetries prevent the sudden formation of singularities at different points in space, as every point is taken to be identical to every other point by fiat. The geometry of these regions is therefore given by the FLRW line-element (23), where $a(t)$ is the scale factor that obeys the Friedmann equation

$$\frac{\dot{a}^2}{a^2} = \frac{8\pi G}{3}\rho - \frac{k}{a^2}, \tag{32}$$

where $\rho \propto a^{-3}$ is the energy density of the dust. In the vacuum regions we will take the geometry to exhibit translational symmetry along the line of sight, but will not restrict the geometry to be FLRW, as it is known that no solutions that satisfy the junction conditions will exist in this case. The geometry of this region is then given by

$$ds^2 = -d\hat{t}^2 + b_1^2(\hat{t}) d\hat{X}^2 + b_2^2(\hat{t}) \left( d\hat{Y}^2 + d\hat{Z}^2 \right), \tag{33}$$

where $b_1(\hat{t})$ and $b_2(\hat{t})$ are the scale factors in the directions tangent and normal to the line of sight, respectively.

It can be shown that the junction conditions between these two regions are satisfied if we identify our hatted and un-hatted coordinates at the boundary, and if $k = 0$, $b_1 = a^{-1/2}$ and $b_2 = a$ [44, 46]. The dust dominated regions are then spatially flat FLRW, the vacuum regions are Kasner, and the entire geometry is an exact solution of Einstein's equations [45]. These solutions are, in fact, a special case of the general dust solution admitting a three dimensional group of space-like Killing vectors on two dimensional planar subspaces [23, 63], but are chosen such that we can have collapsing regions that do not exhibit the shell crossing singularities that tend to rapidly form in the general case. We can arrange for either the dust regions to be collapsing and the vacuum regions to be expanding along the line of sight, or the dust regions to be expanding and the vacuum regions to be collapsing along the line of sight. Here we will concentrate on the former, which appears to us to be more in-keeping with the usual picture of what is expected to happen in the late Universe (voids expanding, and dense regions collapsing).

In order to calculate observational quantities within this solution, along our chosen line of sight, we will need to specify a set of observers. In the dust dominated regions these can be conveniently chosen to be comoving with the fluid, such that they follow a set of geodesic curves with tangent vector $u^a = (1, 0, 0, 0)$. In the vacuum regions we will also take our observers to follow curves with tangent vector $u^a = (1, 0, 0, 0)$, in the coordinates used in Eq. (33). One should note that although there is no fluid in this case, so that this choice is not unique, it is a choice that picks out a set of curves that are parallel to the world-lines of observers who stay at the boundary between regions. They are also geodesic. These choices therefore correspond to a congruence of complete geodesic curves that fill the entire spacetime.

Let us again refer to the dust dominated regions as Region I and the vacuum regions as Region II. Null geodesic curves in these two regions, in the direction of the inhomogeneity, are given by

$$k^a_I = \frac{c_1}{a^2}\,(a, 0, 0, -1) \tag{34}$$

$$k^a_{II} = c_2\left(\sqrt{a}, 0, 0, -a\right), \tag{35}$$

where $c_1$ and $c_2$ are constants, and where we have again taken the affine parameter that defines these tangents to decrease into the past. The energy of a photon following $k^a$, as measured by the observers following the curves $u^a$, is given by

$$E_I = \frac{c_1}{a} \tag{36}$$

$$E_{II} = c_2 a^{1/2}, \tag{37}$$

where $E = -u_a k^a$. We can also see that the Sachs optical equations in the two regions reduce to

$$\frac{d^2 d_{A,I}}{d\lambda^2} = -\frac{2c_1^2}{3a^5}\,d_{A,I} \tag{38}$$

$$\frac{d^2 d_{A,II}}{d\lambda^2} = 0, \tag{39}$$

where $c_1$ is the constant from Eq. (34), which will be different within each individual dust dominated region. As always, the redshift is given by taking the ratio of photon energy at the time of emission and observation, calculated using Eqs. (36) and (37).

The trajectories of photons can be straightforwardly integrated between the different regions, using Eqs. (34) and (35), and by taking the value of $\hat{X}(\hat{t})$ on leaving one region as its initial value on entering the next. Likewise, the value of $E$ can be calculated along the null trajectories by setting its value on entering one region as being equal to its value on leaving the last. This gives the value of the constants $c_1$ and $c_2$ in each of the dust and vacuum regions respectively, and allows Eqs. (38) and (39) to be integrated along the null trajectory. Integration of this equation again requires setting $d_A$ and $\theta$ to be equal at the boundaries between regions. Following the prescription above, the model is uniquely specified once we specify three pieces of information: (i) The size of the vacuum regions, (ii) the size of the dust regions, and (iii) the time until the dust regions reach the 'big crunch'.

Now let us consider the Buchert average of this geometry. The usual procedure is to average the expansion scalar over a space-like hypersurface, and use the averaged value to calculate observables. Here we have created a model that is inhomogeneous in one direction only. Averaging in all three spatial directions should *not* therefore be expected to reproduce anything like the observations we can calculate by looking in the direction of the inhomogeneity. Instead, we consider that the appropriate thing to do (and in analogy to the case of inhomogeneity in all 3 spatial directions), is to average the scale factor in the direction of inhomogeneity only. We are then left with an averaged geometry with line-element

$$ds^2 = -dt^2 + \langle b\rangle^2\,dX^2 + a^2(t)\left(dY^2 + dZ^2\right), \tag{40}$$

where the averaged scale factor, $\langle b\rangle$, is given by

$$\langle b\rangle = \frac{\int \sqrt{g_{XX}}dX}{\int dX}. \tag{41}$$

We can now calculate observables in this averaged geometry, and compare them to the observations made along the line of sight in the actual geometry of the spacetime.

Let us now consider the spatial average of the local volume deceleration parameter. Again, we do not want to average over all spatial directions, as we are only considering inhomogeneity and observations along one preferred direction. The average of $q_\Theta$ along the line of sight is therefore given by

$$\langle q_\Theta\rangle = \frac{\int q_\Theta\sqrt{g_{XX}}dX}{\int \sqrt{g_{XX}}dX}, \tag{42}$$

where $q_\Theta$ is $1/2$ in the collapsing dust regions, and $-4$ along the $X$-direction in the vacuum regions. We find a similar expression for $q_{\rm KS}$, which takes the same value as $q_\Theta$ in both the dust and vacuum regions.

### C. Lemaître-Tolman-Bondi model

In the previous two sections, we considered models consisting of alternating expanding vacuum and collapsing dust regions. We will now consider a model with no discontinuities in the density distribution, in the form of the spherically-symmetric, dust-only Lemaître–Tolman–Bondi (LTB) solutions [48–50]. These have been the focus of much recent interest due to their ability, in the guise of 'giant void' models, to reproduce the observed supernova Hubble diagram without a cosmological constant [64–70]. They are also capable of having an accelerating spatial average under certain conditions [71–74].

The LTB metric is given by

$$ds^2 = dt^2 - \frac{a_2^2(t,r)}{(1-k(r)r^2)}dr^2 - a_1^2(t,r)r^2 d\Omega^2, \qquad (43)$$

where $a_2 = (a_1 r)'$ is the radial scale factor. The transverse scale factor $a_1$ must satisfy the analogue of the Friedmann equation,

$$\left(\frac{\dot{a}_1}{a_1}\right)^2 = \frac{8\pi G}{3}\frac{m(r)}{a_1^3} - \frac{k(r)}{a_1^2} + \frac{\Lambda}{3}. \qquad (44)$$

Primes and over-dots denote partial derivatives with respect to $r$ and $t$, respectively. The functions $k(r)$ and $m(r)$ are arbitrary functions of the radial coordinate, and may be interpreted as the spatial curvature and a mass density at a given radius. The sign of $k(r)$ classifies the differential equation, and analytic parametric solutions exist for each sign. Integrating Eq. (44) with respect to time introduces a third arbitrary radial function, $t_B(r)$, which describes the local time since the big bang singularity along the world-lines of the dust.

The metric in Eq. (43) is invariant under the transformation $r \to f(r)$, which can therefore be used to set one of the arbitrary functions to a simple form, without losing any generality. The LTB solutions are isotropic about $r = 0$ only, and in general have different expansion rates in the radial and transverse directions ($H_1 = \dot{a}_1/a_1$ and $H_2 = \dot{a}_2/a_2$, respectively). The density, expansion, and shear scalars for this spacetime are

$$\begin{aligned} \rho &= \frac{(mr^3)'}{3a_2 a_1^2 r^2} && (45)\\ \Theta &= 2H_1 + H_2 && (46)\\ \sigma^2 &= \frac{1}{3}(H_1 - H_2)^2. && (47) \end{aligned}$$

Observers away from the centre of symmetry have anisotropic distance-redshift relations, in general. Rather than solving the Sachs equations in full for every direction on the sky, we will operate within the *dipole approximation*[2], which assumes that the dipole term dominates the anisotropy of the distance-redshift relation [75–78]. The dipole is aligned with the radial direction due to the symmetry of the model, and so the monopole can be estimated by taking the mean of the angular diameter distance in the radial directions facing into and out from the centre of symmetry,

$$d_A(z)|_{\ell=0} \approx \frac{1}{2}[d_A(+\hat{r},z) + d_A(-\hat{r},z)]. \qquad (48)$$

We expect this to be a reasonable approximation for the models considered here. The observational deceleration parameter, $q_{\rm obs}$, is defined using the monopole of $d_A$ only.

For light propagation purely in the radial direction, the tangent vector to the null geodesics is

$$k^a = \left((1+z), \pm\frac{\sqrt{1-kr^2}}{a_2}(1+z), 0, 0\right), \qquad (49)$$

and the redshift is given by integrating

$$\frac{dz}{d\lambda} = -H_2(1+z)^2. \qquad (50)$$

The angular diameter distance in either direction can be found using the Sachs equation (9) in the radial direction.

In general, spatial averages in an LTB spacetime will be both position- and domain-dependent. We consider spatial averaging only for spherical domains centred at $r = 0$, on hypersurfaces of constant $t$. We define the effective scale factor to be $a_{\mathcal{D}} = (V_{\mathcal{D}}/V_{\mathcal{D},0})^{\frac{1}{3}}$, where

$$V_{\mathcal{D}} = 4\pi \int_0^{r_{\mathcal{D}}} \frac{a_2 a_1^2 r^2}{\sqrt{1-k(r)r^2}} dr \qquad (51)$$

and $r_{\mathcal{D}}$ is the radius of the spherical domain. The average of a scalar quantity is then given by

$$\langle S \rangle = \frac{4\pi}{V_{\mathcal{D}}} \int_0^{r_{\mathcal{D}}} S(r,t) \frac{a_2 a_1^2 r^2}{\sqrt{1-k(r)r^2}} dr. \qquad (52)$$

We consider only the class of LTB models with $\Lambda = 0$. This means that the spacetime is locally decelerating everywhere, $q_\Theta \geq 0$. The Kristian-Sachs measure is also necessarily decelerating ($q_{\rm KS} \geq 0$).

Nevertheless, the freedom in the radial profiles makes it possible to construct models in which the Hubble diagram exactly matches that of an accelerating FLRW model for $z > 0$, as seen by an observer at the centre of symmetry (although see [79]). As a result, LTB models have been studied extensively as a conventional relativistic explanation of the apparent acceleration inferred from supernova observations which does not require the existence of an exotic dark energy component, or modifications to the theory of gravity (e.g. [55, 64–66, 77, 80–85]). Despite some success, however, they ultimately seem unable to account for certain combined sets of cosmological observables[3] [77].

Acceleration of the Buchert average, $q_{\mathcal{D}} < 0$, has been demonstrated for a number of different LTB models (e.g. [71–73, 86, 87]). The cases studied generally take spherical averaging domains, centred about the origin. They typically find acceleration only for finite ranges of domain size, which do not correspond to the homogeneity scale (if one exists). Additionally, models in which observers at the centre of symmetry infer acceleration from their Hubble diagram seem not to correspond to those with an accelerating Buchert average [71], and vice versa

---

[2] See the end of Section VI, and reference [75], for a discussion of the validity of this approximation.

[3] For an alternative perspective, see [30].

[88]. Since the spacetime is always decelerating locally, the existence of acceleration in the Buchert average must be caused purely by the backreaction term, Eq. (20).

In what follows, we will specialise to LTB models with a simple Gaussian spatial curvature profile

$$k(r) = A_k \exp\left(-\frac{r^2}{w_k^2}\right), \tag{53}$$

with $t_B$ =constant, and with a choice of radial coordinate such that $m(r)$ =constant. When $A_k < 0$, there is a central void region (often surrounded by an over-dense shell), and an asymptotic flat FLRW region. These models are capable of producing good fits to the existing supernova data, for an observer at the centre of symmetry.

## IV. RESULTS: SPHERICAL COLLAPSE

In this section, we evaluate our 4 measures of acceleration in the spherical collapse model (as described in Section III A). This model is known to be able to have an accelerating Buchert average, despite locally decelerating everywhere [7].

In Figure 2 we plot the magnitude of sources, $\mu$, that an observer in the spherical collapse model would see, minus the magnitude a source at the same redshift would have in a pure vacuum model (with all of the dust regions removed). The model used in this figure is one in which the vacuum regions are 80 Mpc wide at the present time, and dust regions are 15 Mpc wide. We refer to these plots as 'the Hubble diagram'. We consider two different observers in this plot: one at the centre of a collapsing dust region (red line), and one at the centre of an expanding vacuum region (blue line). It can be seen that the type of region that the observer finds themselves in can have a considerable impact on the behaviour of the Hubble diagram they construct at low $z$. At high $z$, however, the curves evolve almost identically (up to a vertical displacement). In both cases, the blueshifting that occurs in the collapsing region forces the curves upwards, due to the magnitude continuing to increase even while the redshift decreases. This leads to an overall positive gradient for the curves in Figure 2, while the gradient at any point on each individual curve is negative. This result is significant, as accelerating FLRW models have positive gradient in these plots, while decelerating FLRW models have negative gradient.

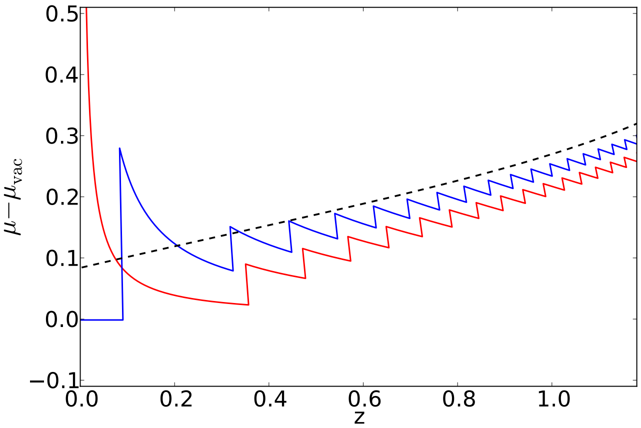

Figure 2: Magnitude of sources in the spherical collapse model, minus the magnitude they would have in pure vacuum. Observations made by a single observer, from the centre of the dust and vacuum regions, are displayed as solid red (lower at $z = 1$) and blue lines, respectively. The dashed black line is the same quantity in the Buchert averaged model.

In Figure 3 we plot the results of averaging the Hubble diagrams constructed by observers in both the dust and vacuum regions of the same model considered in Figure 2. We do this by constructing individual distance-redshift relations for a large number of observers (all in the same model), binning these relations in redshift, and then calculating the mean and standard deviation in each bin. We also calculate the magnitudes that would be found in the Buchert averaged model, and the spatially averaged deceleration parameter $q_\Theta = q_{\rm KS}$. In the upper panel of Figure 3 we plot the magnitude of sources, minus the magnitude they would have at the same redshift if all the dust regions were removed (as in Figure 2). In the lower panel we plot the magnitude of sources minus the magnitude they would have in the Buchert averaged model. In this figure we shift the curves so that they coincide at $z = 0$. This corresponds to a change in the local Hubble rate.

It can be seen from the upper panel of Figure 3 that the Buchert average (dashed black line) closely traces the mean observed magnitude (solid red line). The 1 and $2\sigma$ confidence regions appear to oscillate, because of the jaggedness of the individual distance-redshift curves that were averaged over (see Figure 2). Nevertheless, the curve for the Buchert average stays within the $1\sigma$ confidence region for the entire redshift range considered. Part of the reason for this is that the black line has been shifted vertically to match the red line at high $z$, in order to aid comparison. Without this shift, the two curves have the same zero-point, but fluctuations in the mean observational curve at low $z$ cause an offset to build up at higher $z$. The zero-points are the same because they are governed by the same spatial average of the local Hubble rate $\langle H_0 \rangle$ (for the observational curve) and the Buchert average Hubble rate $H_{\mathcal{D}}$ (for the Buchert average curve). These are equal at $z = 0$.

It can be seen from the lower panel in Figure 3 that making the comoving size of the regions smaller, so that the initial region is less dominant, significantly reduces the fluctuations of the mean observational curve (in both cases, these fluctuations decrease as redshift increases). This in turn reduces the offset that develops between the observational curve and the Buchert average curve.

The short blue line in the upper panel of Figure 3 is the 'effective' curve obtained by setting $q_0 = \langle q_\Theta \rangle$ in the FLRW series expansion for $d_A(z)$. Again, $q_\Theta = q_{\rm KS}$ in the

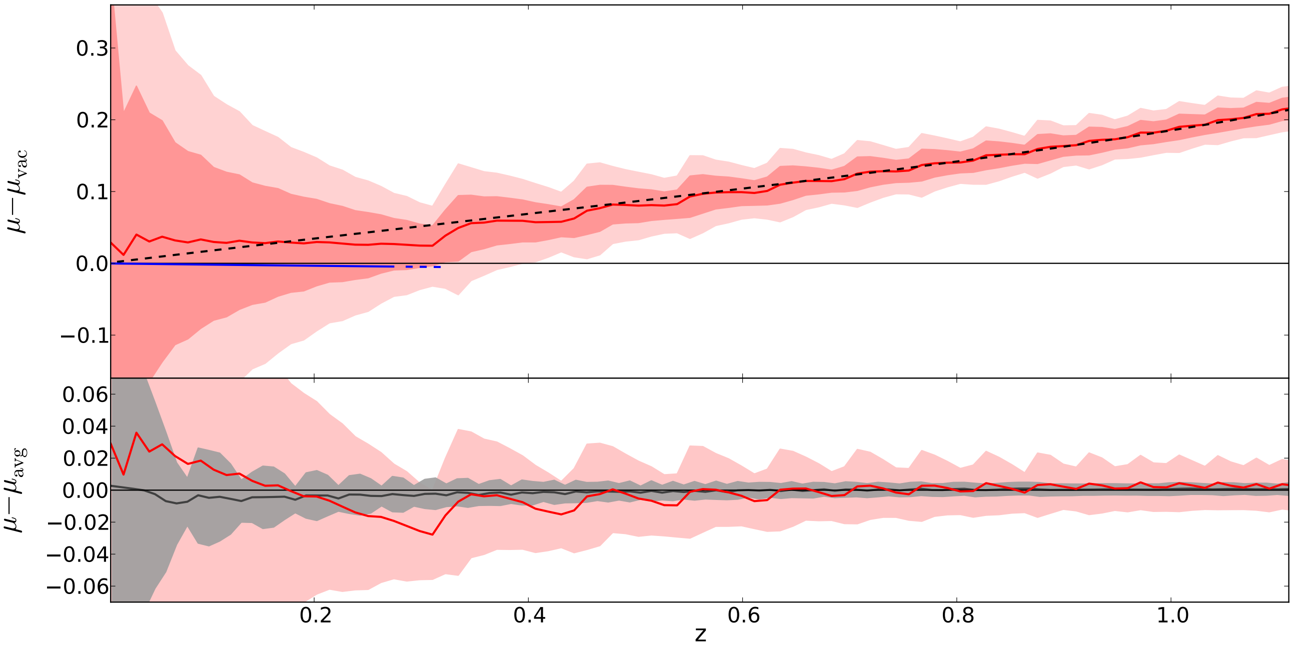

Figure 3: Upper Panel: Magnitude of sources in the spherical collapse model, minus the magnitude they would have in pure vacuum. The solid red line is the mean observed magnitude, obtained by spatially averaging distance-redshift relations on a surface of $t$ =constant. The pink bands are $1\sigma$ and $2\sigma$ confidence regions. The black dashed line shows the corresponding quantity in the Buchert averaged model. The short blue line is the distance modulus for a FLRW model with deceleration parameter $q = \langle q_\Theta \rangle$. Lower Panel: A difference plot of the red line and dashed line, from the panel above. The solid black line corresponds to a model with regions that are a quarter of the size of those used in the upper panel. The pink (wide) and grey (narrow) bands are $1\sigma$ confidence regions for the two different models.

spherical collapse model, so this line is also the effective curve for the Kristian-Sachs deceleration parameter. It can be seen to bear little resemblance to the observational and Buchert average curves.

The values for the deceleration parameters measured in this model are

$$\langle q_\Theta \rangle \simeq 0.017 \tag{54}$$

$$q_{\mathcal{D}} \simeq -0.167, \tag{55}$$

with $\langle q_{\rm KS} \rangle = \langle q_\Theta \rangle$, and $\langle q_{\rm obs} \rangle \simeq q_{\mathcal{D}}$. By considering other model parameters, we have confirmed that the curves due to averaging observations, and the Buchert average distance curve, always seem to show similar functional behaviour (and thus have similar deceleration parameters). Neither of these quantities are ever close to $\langle q_{\rm KS} \rangle$ or $\langle q_\Theta \rangle$, unless the dust regions are made to expand, or are made to be very small.

We find that the existence of acceleration in both the Buchert average and the observational distance-redshift relations is a generic feature of spherical collapse models consisting of expanding and collapsing regions. Figure 4 shows the results of varying the parameters of the FLRW regions that constitute the model. The base model has the parameters $h_I = -2.0$ and $\Omega_{m,I} = 1.8$ in the dust regions, and $h_{II} = 0.7$ and $\Omega_{m,II} = 0$ in the vacuum regions. The comoving sizes of these regions are taken to be $\chi_I = 15$ Mpc and $\chi_{II} = 80$ Mpc, respectively. The collapsing region is chosen to be 52% of its maximum age. The plots in Figure 4 are for models with these parameter values, unless they are the parameter being varied. The figure shows a strong dependence of the Buchert average acceleration on region size – models with collapsing regions that are relatively larger have greater acceleration, as expected. Increasing the Hubble rate in the vacuum regions reduces the current age of the model, and correspondingly increases $\langle q_\Theta \rangle$. This is due to this quantity being evaluated at an earlier time, when the collapsing regions are more dominant. Figure 4 shows that the deceleration parameter of the Buchert averaged model is negative as long as the collapsing region takes up a non-negligible fraction of the comoving volume. If the vacuum region dominates, both the local volume and Buchert average deceleration parameters tend to zero. Since the observational deceleration parameter is well-approximated by the Buchert average measure, it seems that all that is required for observers to see an apparent acceleration is the existence of a non-negligible fraction of collapsing regions.

## V. RESULTS: KASNER-EDS

We now repeat the analysis of the previous section for the Kasner-EdS model. This is included in order to al-

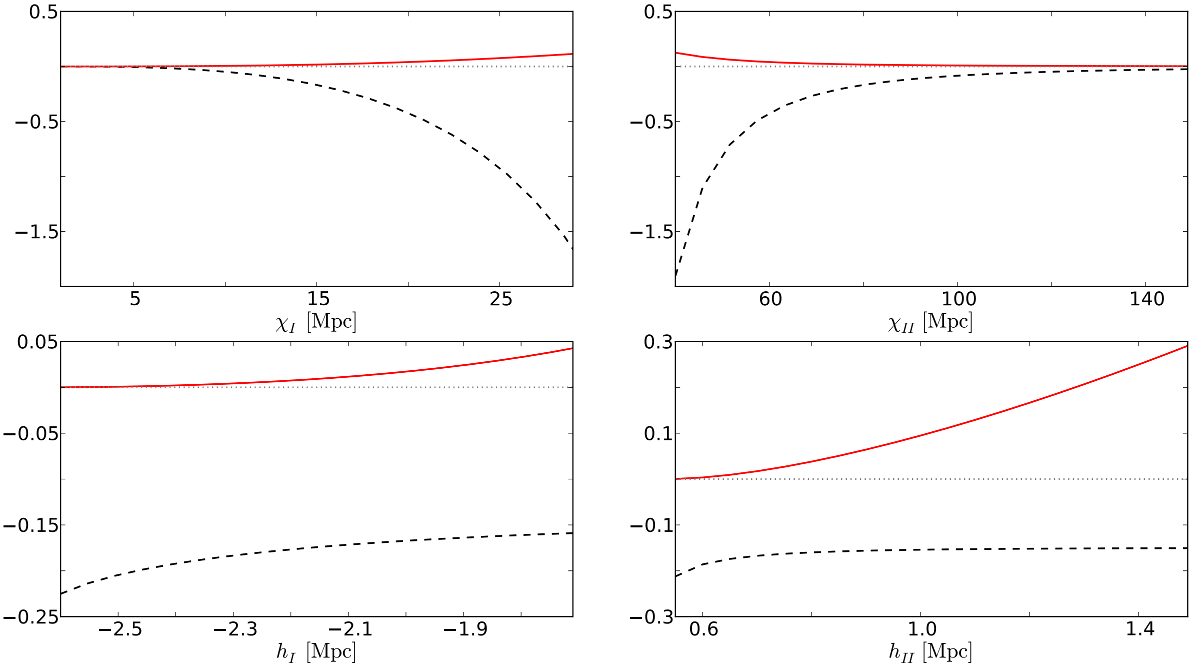

Figure 4: Dependence of the Buchert average deceleration parameter, $q_{\mathcal{D}}$ (dashed black line), and spatially-averaged local volume deceleration parameter, $\langle q_\Theta \rangle$ (solid red line), on the parameters of the spherical collapse model. Shown is the dependence on the Hubble rates in the collapsing and vacuum regions, $h_I$ and $h_{II}$, and the comoving region sizes, $\chi_I$ and $\chi_{II}$.

lay concerns that the coherence in the accelerations of the Buchert average and observational measures seen in the spherical collapse model were caused simply by inadequacy of the model.

In Figure 5 we plot the magnitude of sources, $\mu$, that an observer in the Kasner-EdS model would see, minus the magnitude a source at the same redshift would have in a pure vacuum model (with all of the dust regions removed). The model used in this figure again has dust regions that are 15 Mpc wide, but the vacuum regions are now $\sim$ 1500 Mpc across. This large number is required in order to get cosmologically interesting redshifts, because of the rapid acceleration in the vacuum regions along the preferred line of sight[4]. We also choose the model such that the dust regions collapse to a singularity in $\sim$ 5 billion years. We consider two different observers in Figure 5: one at the centre of a collapsing dust region (green line), and one at the centre of an expanding vacuum region (blue line). Again, it is apparent that the type of region that the observer finds themselves in can have a considerable impact on the behaviour of the Hubble diagram they construct at low $z$, while at high $z$ the curves evolve almost identically (up to a vertical displacement). Blueshifting again occurs in the collapsing regions, forcing the curves upward.

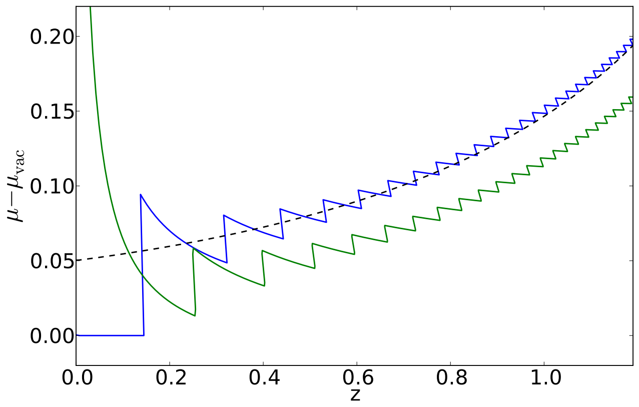

Figure 5: The same quantities that were plotted in Figure 2, but using the Kasner-EdS model.

In Figure 6 we plot the results of averaging the distance-redshift relations of observers in both the dust

---

[4] It should be reiterated here that we are not proposing this model as a realistic representation of the actual Universe, but rather to provide a simple exact solution of Einstein's equations that allows us to study relativistic behaviour that may occur in more realistic solutions. In this sense, it should be considered as proof-of-concept only.

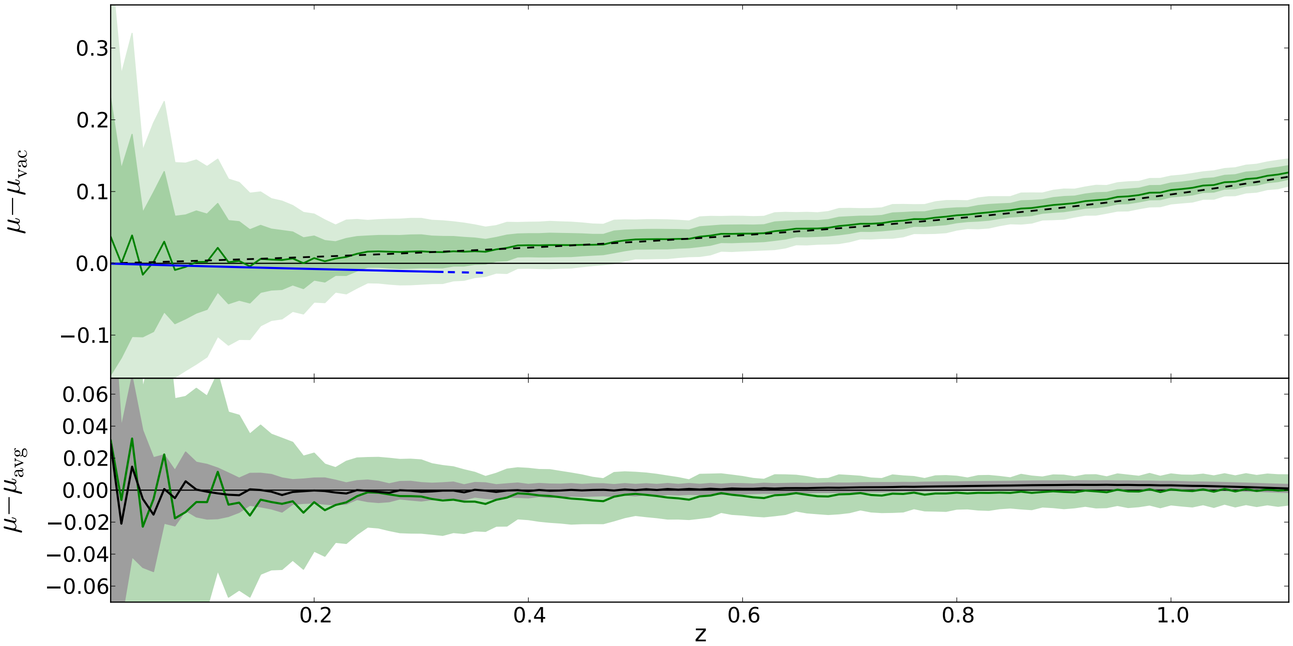

Figure 6: The same quantities that were plotted in Figure 3, but using the Kasner-EdS model.

and vacuum regions of the same model considered in Figure 5, as was done in Figure 3 for the spherical collapse model. Magnitudes in the Buchert averaged model, and the spatially averaged deceleration parameter $q_\Theta = q_{\rm KS}$, are also calculated. With this model, however, no vertical shift of the Buchert averaged model curve is required in order for it to agree well with the average of the observed magnitudes. The Buchert average closely traces the mean observed magnitudes. We do, however, perform a vertical shift on all of the curves in Figure 6 simultaneously, so that they approach the origin at $z = 0$. Again, reducing the comoving size of the regions, so that the initial region is less dominant, significantly reduces the fluctuations of the mean observational curve.

The short blue line in the upper panel of Figure 6 is again the 'effective' distance modulus curve obtained by setting $q_0 = \langle q_\Theta \rangle$ in the FLRW series expansion for $d_A(z)$. We also again have $q_\Theta = q_{\rm KS}$. The values for the deceleration parameters measured in this model are

$$\langle q_\Theta \rangle \simeq -3.96 \tag{56}$$

$$q_{\mathcal{D}} \simeq -7.18, \tag{57}$$

with $\langle q_{\rm KS} \rangle = \langle q_\Theta \rangle$, and $\langle q_{\rm obs} \rangle \simeq q_{\mathcal{D}}$. This value of $\langle q_\Theta \rangle$ corresponds to rapid acceleration, but not as rapid as simply looking through pure vacuum regions in the direction of inhomogeneity, where $q_0 = -4$. The value of $q_{\mathcal{D}}$, on the other hand, corresponds to considerably more acceleration than simply looking through the vacuum regions alone. As in the spherical collapse models, therefore, the presence of the collapsing dust regions causes a dramatic increase in both the acceleration of the Buchert averaged model, and the average of the observational acceleration.

By considering models with other parameter values, we again confirm that the curves due to averaging observations, and the Buchert average distance curve, always seem to show similar functional behaviour (and thus have similar deceleration parameters). Neither of these quantities are ever close to $\langle q_{\rm KS} \rangle$ or $\langle q_\Theta \rangle$, unless the dust regions are removed, or become vanishingly small.

## VI. RESULTS: LTB

The final model that we consider is an LTB spacetime, with parameters chosen to produce a good fit to the supernova data for an observer at $r = 0$. These are displayed in Figure 7. Unlike the other models we have considered, the LTB model has smooth density and Hubble rate profiles on spatial slices. There are, however, no collapsing regions at $t = t_0$.

Figure 9 displays the magnitudes of sources in the LTB model for our various measures of acceleration. Since the chosen model has no homogeneity scale, we plot the distance modulus curves for two different averaging domain radii: $r_{\mathcal{D}} = 1000$ Mpc (well inside the void), and $r_{\mathcal{D}} = 3000$ Mpc (near the void boundary). The results in the two cases differ significantly, with the smaller averaging domain displaying acceleration for the mean observational curve (solid red line), while its counterpart for the larger domain (solid blue line) shows a strong deceleration. Note that the observational curves are for the *monopoles* of the distance-redshift relation, obtained using the dipole approximation described in Section III C. The curves for the Buchert average (dashed lines) do not

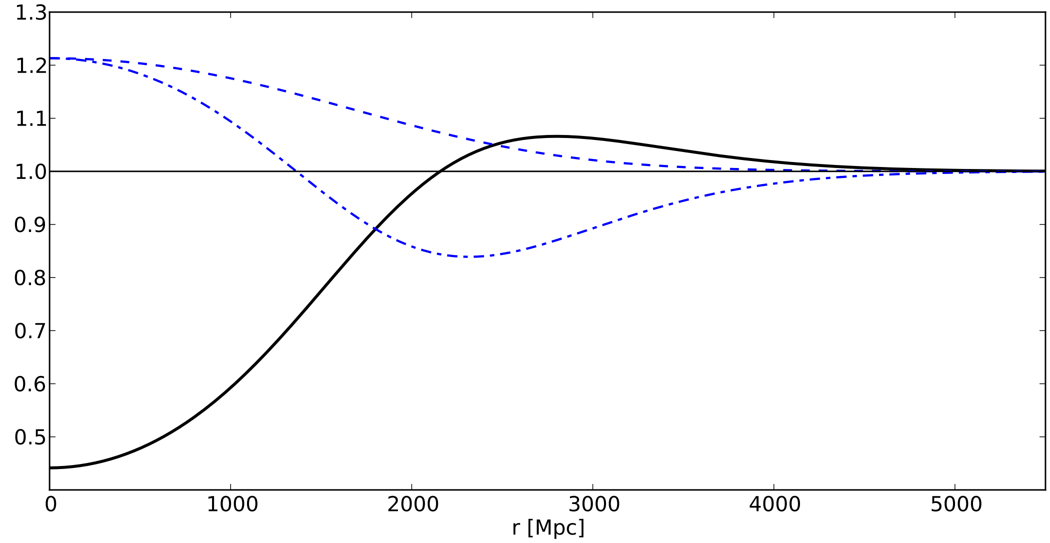

Figure 7: Density and expansion rates as a function of radius in an LTB void model. The model has spatial curvature of the form given in Eq. (53), with $A_k = -3.82 \times 10^{-8}\mathrm{Mpc}^{-2}$ and $w_k = 1800$ Mpc. Shown are the density, $\rho$ (solid black), transverse Hubble rate, $H_1$ (blue dashed), and radial Hubble rate, $H_2$ (blue dash-dot). All of the curves are normalised to their values in the asymptotically-homogeneous region ($\rho = 9.2 \times 10^{10}\mathrm{M}_\odot\mathrm{Mpc}^{-3}$, $H_1 = H_2 = 57.7$ $\mathrm{kms}^{-1}\mathrm{Mpc}^{-1}$).

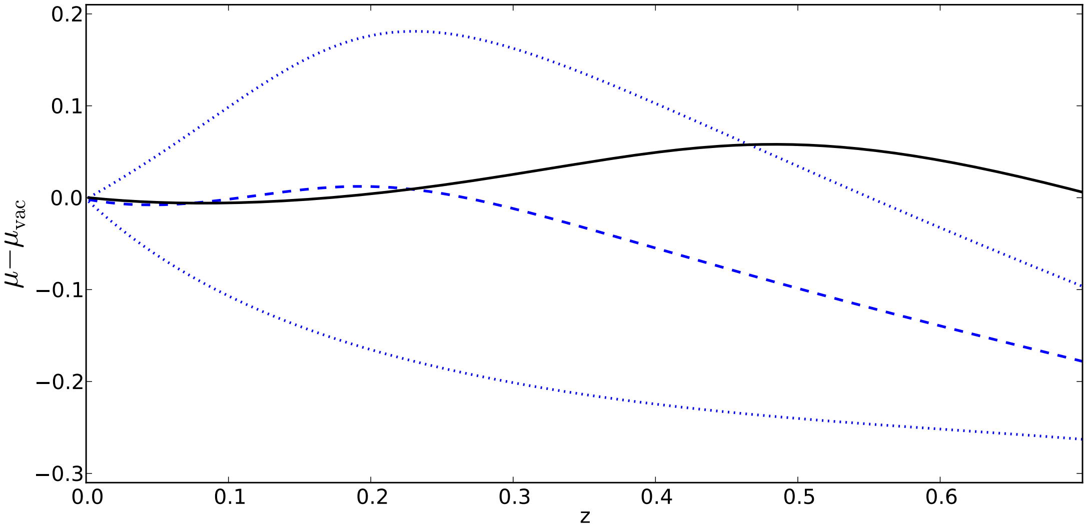

Figure 8: Distance modulus curves for an off-centre observer in the same model, at $r = 915$ Mpc. The dotted blue lines show the distance modulus as a function of redshift for radial lines of sight looking out of and into the void (upper and lower curves respectively). The dashed blue line is the distance modulus for the monopole of the distance-redshift relation, calculated using the dipole approximation. The solid black line is the relation for an observer at the centre of symmetry.

match the mean observational curves (solid lines) in any discernible way. In particular, both of the curves for the Buchert average are decelerating, while the averaged observed relation for the smaller domain size is accelerating.

The dotted and dash-dotted lines are 'effective' distance moduli for the local volume and Kristian-Sachs deceleration parameters. These correspond to series expansions of the FLRW $d_A(z)$ relation with deceleration parameters $q_0 = \langle q_\Theta \rangle$ and $q_0 = \langle q_{\mathrm{KS}} \rangle$ respectively. Neither follows the Buchert average, nor the mean observational curves. They are closely related to one another though, with only a slight discrepancy apparent at higher red-

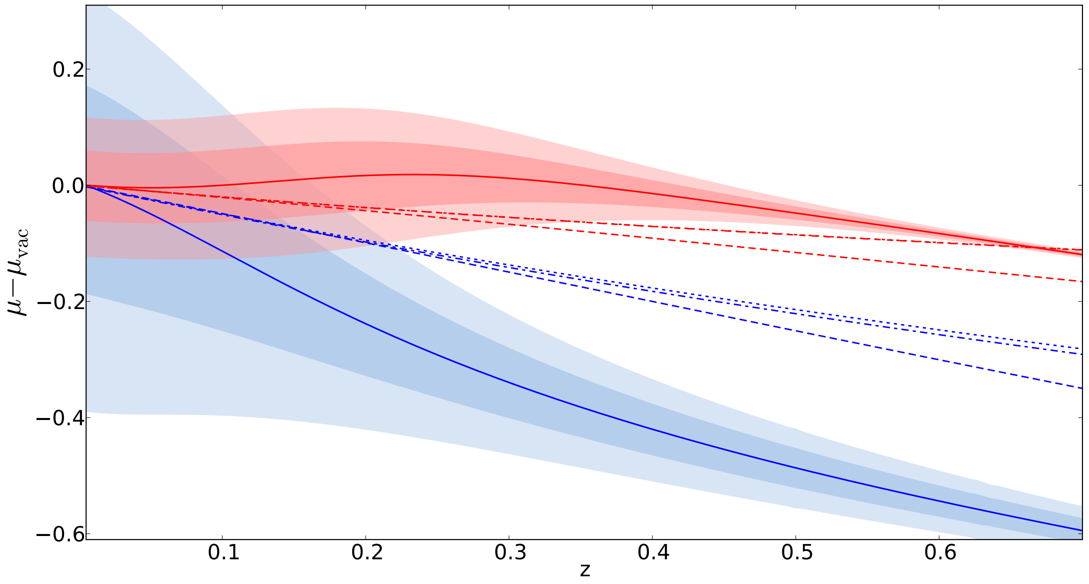

Figure 9: Distance moduli in the LTB model. The red curves (uppermost) are for averaging domains of size $r_{\mathcal{D}} = 1000$ Mpc, and the blue curves for $r_{\mathcal{D}} = 3000$ Mpc. The solid lines are the mean distance moduli found by spatially averaging the monopole of the observed distance-redshift relation, with accompanying $1\sigma$ and $2\sigma$ confidence bands. The dashed lines are the distance moduli for the distance-redshift relation in the Buchert averaged spacetime. The dotted and dot-dashed lines are the distance moduli for a series expansion of the FLRW $d_A(z)$ relation, with deceleration parameters $q = \langle q_\Theta \rangle$ and $q = \langle q_{\rm KS} \rangle$, respectively. The curves have all had their zero-points shifted to match at $z = 0$.

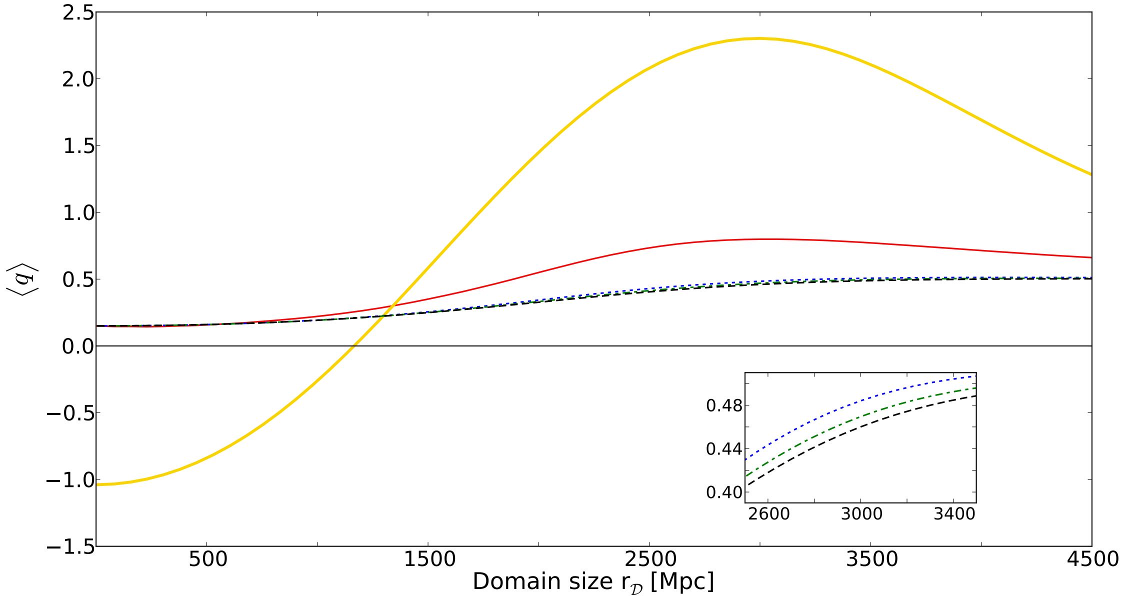

Figure 10: Spatial averages of various deceleration parameters as a function of averaging domain radius, $r_{\mathcal{D}}$. The local volume (dash-dotted green line), Kristian-Sachs (dotted blue), and Buchert average (dashed black) deceleration parameters have rather similar values. A close-up of these curves is shown in the inset so that they can be distinguished. The thick, solid yellow line is the deceleration parameter found by fitting an FLRW model to the distance-redshift relation for a wide range of redshifts, $z \leq 1$. The narrower solid red line shows the same measure, but for a fit to only $z \leq 0.1$.

shift for the larger domain size. This is because the two measures only differ by a term proportional to the shear, which is relatively small in this case.

The upper set of observational curves in Figure 9 show that a substantial fraction of observers within a radius of $r \leq 1000$ Mpc will infer acceleration from the monopole of their Hubble diagram, despite all of the other deceleration parameters indicating deceleration. This is caused by spatial variations in expansion rate along their lines of sight, but does not seem to be linked with spatial average properties of the spacetime, as it was in the spherical collapse and Kasner-EdS models. Fig. 8 suggests that many of these observers will see a large dipole in the distance-redshift relation over their sky. Presumably, most of the observers would conclude that they lived in a Universe that is inhomogeneous on large scales, and would therefore not attempt to fit an FLRW model to their observations at all. In that case, the question of whether the monopole of the observational relation is accelerating or not becomes less of an issue. Attempts to summarise the (observational) acceleration of the model with one number, the monopole $q_{\rm obs}$, would fail. Attempting to construct a homogeneous Buchert average model would probably not be seen as a sensible procedure either[5].

The Buchert average curve in Figure 9 is much closer to the effective local volume acceleration and Kristian-Sachs curves than to the observational curve, although it still deviates from both of them substantially. There are a number of reasons why this is the case. The first is that the model is not statistically homogeneous, and so the Buchert average does not represent the 'typical' conditions that a light ray would experience traveling through the spacetime[6]. Secondly, the backreaction scalar $\mathcal{Q}_{\mathcal{D}}$, of Eq. (20), is small in this model, because both the shear and the variance of the expansion rate are small. As such, the Buchert average deceleration parameter $q_{\mathcal{D}}$, defined in Eq. (21), is dominated by the same terms that appear in the definitions of the Kristian-Sachs and local volume measures, most notably the density. Our different measures of acceleration do not *exactly* reduce to one another in this case, but they are rather close (as can be seen in Figure 10, inset). We also see that in the absence of a sensible way of defining a representative smooth model (due to the lack of a homogeneity scale), the mean behaviour of light rays should not be expected to correspond to the Buchert averaged model.

In Figure 10, the various (spatially-averaged) deceleration parameters are plotted as a function of averaging domain radius, $r_{\mathcal{D}}$. The Buchert average, local volume, and Kristian-Sachs deceleration parameters track one another rather closely over the whole range of domain sizes, for the reasons discussed above. The observational curves (thick and thin solid lines) have a rather different behaviour. Both are obtained by calculating $q_0$ in an FLRW model that has been fit to the monopole of the distance-redshift relation as a function of observer position[7]. The resulting position-dependent value of $q_0(r)$ is then spatially averaged. The thick yellow curve corresponds to fitting FLRW models to the distance-redshift monopole out to $z = 1$, and the thin red one to $z = 0.1$. The two are very different. In particular, the fit out to higher redshifts shows acceleration for small averaging domain radii. Figure 8 shows why this is the case: At low redshift, the observational distance modulus curve is decelerating (which is also suggested by the fact that $q_{KS} > 0$ everywhere), but appears to accelerate at higher redshifts for observers inside the void. By fitting FLRW models to the larger redshift range, more of the apparent acceleration is captured. This behaviour is wholly due to quantities being integrated along past null directions, and is not caused by the local curvature of spacetime at any one point.

The results we have presented for the observational deceleration are subject to the validity of the dipole approximation, that was discussed in Section III C. This approximation will tend to overestimate the monopole of the angular diameter distance at a given redshift, causing a decrease in $q_{\rm obs}$ relative to its exact value. As can be seen from Figure 10, this only serves to worsen the discrepancy between $\langle q_{\rm obs} \rangle$ and the other deceleration parameters at high redshift. At low redshift the approximation is most accurate [76], and so the correction required in this regime should be expected to be small. As such, we consider our results to be robust to the use of this approximation.

## VII. DISCUSSION

In this paper, we have studied different concepts of what it means for a spacetime to display 'accelerating expansion'. The measures of acceleration that are associated with these concepts all reduce to the same quantity in a perfectly homogeneous and isotropic FLRW universe, but in an inhomogeneous universe we have shown that they can be very different indeed. This occurs even to the extent that some can indicate deceleration, while others indicate that exactly the same spacetime is accelerating. In universes that are statistically homogeneous on large scales, we find, that in order to estimate the acceleration inferred by making observations over large distances (as is the most usual way to infer acceleration in cosmology), one is best off using a model constructed from non-local averages of geometric quantities, as occurs in Buchert's formalism, rather than considering the local expansion rate of space. This is in agreement with an argument put forward by Räsänen [89, 90]. The appearance of acceleration in observations made over large scales does not necessarily imply or require the expansion of space to be accelerating, nor does it require local observables to indicate acceleration.

---

[5] Instead, the Buchert averaging procedure could be used to define a 'smoothed-out' model that is inhomogeneous. This would result in position-dependent average quantities, and would likely be sensitive to both the shape and size of the averaging domain.

[6] In fact, it cannot, as the null geodesics involved in calculating this quantity go outside of the averaging domain.

[7] The best-fit FLRW model may not always be a particularly good fit – the monopole of the distance-redshift relation in LTB models can take on much more complicated functional forms than are allowed in FLRW.

The models that we used to reach these conclusions are given in Section III, and include both exact and approximate relativistic toy models that are known to display some of the types of acceleration we have considered. To be specific, we consider: (A) an approximate 'spherical collapse' model (with disjoint collapsing and expanding FLRW regions); (B) an exact Kasner-EdS model (with expanding and collapsing regions along the line of sight); and (C) an exact LTB model (expanding everywhere). The spherical collapse model has the advantage of being able to model reasonably complicated distributions of matter, while the Kasner-EdS model allows one to model a universe that is statistically homogeneous along the line of sight.

In the spherical collapse and Kasner-EdS models, the reconstructed distance-redshift relation, which corresponds most closely to what is actually measured in observational cosmology, is closely related to the Buchert average, and not the mean local properties of the spacetime. This means that showing that local spacetime cannot accelerate without $\Lambda$, or a quintessence field, is not sufficient to disprove backreaction as a source for the apparent late-time accelerating expansion of the Universe [7, 8]. This does not, of course, mean that the observed acceleration can currently be said to be due to backreaction: the situations we considered here are very much toy models (albeit ones that we expect to capture some of the properties of the real Universe). More study is required and, in particular, more realistic, non-perturbative models of the Universe are required, before any definite conclusions can be drawn about the real Universe. One recent attempt at constructing such models appears to show some evidence of the effects we describe here [91], but it is still neither conclusive nor fully realistic.

As a corollary of our study, a possible source of observational evidence for the hypothesis that the apparent acceleration of the Universe is due to inhomogeneity presents itself: If the parameters of FLRW models inferred from local observations are significantly different from those inferred from observations made over large distances, then this would seem to imply that the FLRW model that we use to model local spacetime is different to the FLRW model that best describes the evolution of the Universe on large scales. Any such difference would signal a significant departure from the predictions of the concordance $\Lambda$CDM model of the Universe, and would therefore cast considerable doubt on the detection of $\Lambda \neq 0$. Of course, inferring cosmological parameters from observations made on small scales is a considerable challenge. Sample variance due to the presence of local structures, and the peculiar velocities they induce, would have to be very well-understood. Nevertheless, the supposed detection of the 'Hubble Bubble' [92] suggests that it may not be entirely impossible.

The link we have found between observations and the spatial average can be explained by considering that, for a large enough collection of null rays, the typical conditions experienced by a ray at a given time, $t$, are likely to correspond to the average of local conditions on a hypersurface of $t$ =constant. These averages are exactly what Buchert's approach is constructed to estimate. As long as spacetime is statistically homogeneous and isotropic above some scale, the result then follows (assuming observers and sources are distributed in a volume-weighted way). These issues have been considered in detail in [38].

In the case of the LTB model, in Section VI we found that the Buchert average was more closely related to the local measures than to the typical distance-redshift relation of an observer, apparently in contradiction with our previous results. This model, however, is not statistically homogeneous or isotropic, and shows apparent (observational) acceleration only for a limited range of averaging domain sizes. Furthermore, the distance-redshift relation is only poorly represented by its monopole alone, since the dipole of the relation would certainly be important too. Therefore, our conclusions are that in this case the Buchert average is not enough to characterise the 'typical' properties of the spacetime, and the mean of the monopole of the distance-redshift relation is also not enough to characterise what a typical observer should expect to see. This leads one to question what it really means for an LTB model to exhibit 'average acceleration' at all.

**Acknowledgements:** We acknowledge the STFC and the BIPAC for support, and A. Coley, C. Clarkson, P. G. Ferreira, S. Räsänen, and O. Umeh for helpful discussions. We are particularly grateful to K. Bolejko for a thorough reading of the manuscript, and to the General Relativity and Cosmology group at Dalhousie University for their hospitality while part of this work was carried out. The computer code used in this paper is available online at `www.physics.ox.ac.uk/users/bullp/`.

[1] Hirata, C. M. & Seljak, U., *Phys. Rev. D* **72**, 083501 (2005).

[2] Clarkson, C. & Umeh, O., *Class. Quantum Grav.* **28**, 164010 (2011).

[3] Kristian, J. & Sachs, R. K., *Astrophys. J.* **143**, 379 (1966).

[4] Buchert, T. & Räsänen, S., *Annual Review of Nuclear and Particle Science HIP-2011-35/TH*, (2011)

[arXiv:1112.5335].

[5] Buchert, T., *Gen. Rel. Grav.* **32**, 105 (2000).

[6] Buchert, T., *Gen. Rel. Grav.* **33**, 1381 (2001).

[7] Ishibashi, A. & Wald, R. M., *Class. Quant. Grav.* **23**, 235 (2006).

[8] Green, S. R. & Wald, R. M., *Phys. Rev. D* **83**, 084020 (2011).

[9] Kolb, E. W. *et al.*, *Phys. Rev. D* **71**, 023524 (2005).

[10] Paranjape, A., Thesis (2009) [arXiv:0906.3165].

[11] Kasai, M., Asada, H., & Futamase, T., *Prog. Theor. Phys.* **115**, 827 (2006).

[12] Räsänen, S., *Phys. Rev. D* **81**, 103512 (2010).

[13] Flanagan, E. E., *Phys. Rev. D* **71**, 103521 (2005).

[14] Geshnizjani, G., Chung, D. J. H., & Afshordi, N., *Phys. Rev. D* **72**, 023517 (2005).

[15] Weinberg, S., *Astrophys. J.* **208**, L1 (1976).

[16] Bonvin, C., Durrer, R., & Gasparini, M. A., *Phys. Rev. D* **73**, 023523 (2006) (Erratum: *Phys. Rev. D* **85**, 029901 (2012)).

[17] Baumann, D. *et al.*, (2010) [arXiv:1004.2488].

[18] Enqvist, K., Hotchkiss, S., & Rigopoulos, G., *JCAP* **03**, 026 (2012).

[19] Rigopoulos, G. & Valkenburg, W., (2012) [arXiv:1203.2796].

[20] Ellis, G. F. R. & Jaklitsch, M. J., *Astrophys. J.* **346**, 601 (1989).

[21] Mattsson, M. & Mattsson, T., *JCAP* **10**, 021 (2010).

[22] Meures, N. & Bruni, M., *Mon. Not. Roy. Astron. Soc.* **419**, 1937 (2012).

[23] Di Dio, E., Vonlanthen, M., & Durrer, R., *JCAP* **1202**, 036 (2012).

[24] Szybka, S. J., *Phys. Rev. D* **84**, 044011 (2011).

[25] Brouzakis, N., Tetradis, N., & Tzavara, E., *JCAP* **02**, 013 (2007).

[26] Vanderveld, R. A., Flanagan, E. E., & Wasserman, I., *Phys. Rev. D* **78**, 083511 (2008).

[27] Bolejko, K. & Célérier, M-N., *Phys. Rev. D* **82**, 103510 (2010).

[28] Clifton, T. & Zuntz, J., *Mon. Not. Roy. Astron. Soc.* **400**, 2185 (2009).

[29] Bolejko, K. & Lasky, P., *Mon. Not. Roy. Astron. Soc.* **391**, L59 (2008).

[30] Clarkson, C. & Regis, M., *JCAP* **02**, 013 (2011).

[31] Marra, V. & Pääkkönen, M., *JCAP* **01**, 025 (2012).

[32] Lindquist, R. W. & Wheeler, J. A., *Rev. Mod. Phys.* **29**, 432 (1957) (Erratum: *Rev. Mod. Phys.* **31**, 839 (1959)).

[33] Clifton, T. & Ferreira, P. G., *Phys. Rev. D* **80**, 103503 (2009).

[34] Räsänen, S., *Proceedings of the July 2008 CRAL-IPNL conference "Dark Energy and Dark Matter"*, (2008) [arXiv:0811.2364].

[35] Kantowski, R., Vaughan, T., & Branch, D., *Astrophys. J.* **447** 35 (1995).

[36] Räsänen, S., *JCAP* **11**, 003 (2006).

[37] Räsänen, S., *Int. J. Mod. Phys. D* **15**, 2141 (2006).

[38] Räsänen, S., *Proceedings of the "Beyond the Concordance Model" workshop*, Stellenbosch Institute for Advanced Study, 23-27 August 2010 [arXiv:1012.0784].

[39] Kolb, E. W., Marra, V., & Matarrese, S., *Phys. Rev. D* **78**, 103002 (2008).

[40] Paranjape, A. & Singh, T. P., *JCAP* **03**, 023 (2008).

[41] Brown, I. A., Robbers, G., & Behrend, J., *JCAP* **04**, 016 (2009).

[42] Li, N., *Cosmological backreaction: from the local Hubble expansion rate to dark energy*, Bielefeld (Germany), Thesis (2008).

[43] Dyer, C. C., Landry, S., & Shaver, E. G., *Phys. Rev. D* **47**, 1404 (1993).

[44] Lake, K., *Astrophys. J.* **401**, L1 (1992).

[45] Landry, S. & Dyer, C. C., *Phys. Rev. D* **56**, 3307 (1997).

[46] Dyer, C. C. & Oliwa, C., *Class. Quant. Grav.* **18**, 2719 (2001).

[47] Hellaby, C., *JCAP* **01**, 043 (2012).

[48] Lemaître, G., *Ann. Soc. Sci. Brussels* **A53**, 51 (1933) (reprinted in *Gen. Rel. Grav.* **29**, 641 (1997)).

[49] Tolman, R. C., *Proc. Nat. Acad. Sci. USA* **20**, 169 (1934) (reprinted in *Gen. Rel. Grav.* **29**, 935 (1997)).

[50] Bondi, H., *Mon. Not. Roy. Astron. Soc.* **107**, 410 (1947).

[51] Ellis, G. F. R., Relativistic Cosmology. In: Sachs, R. K. (ed), *General Relativity and Cosmology, Proc. Int. School of Physics "Enrico Fermi" (Varenna), Course XLVII.* Academic Press, New York (1971) (reprinted in *Gen. Rel. Grav.* **41**, 581 (2009)).

[52] Visser, M., *Class. Quant. Grav.* **21**, 2603 (2004).

[53] Etherington, I. M. H., *Phil. Mag.* **15**, 761 (1933) (reprinted in *Gen. Rel. Grav.* **39**, 1047 (2007)).

[54] Clarkson, C. & Maartens, R., *Class. Quantum Grav.* **27**, 124008 (2010).

[55] Clifton, T., Ferreira, P. G., & Land, K., *Phys. Rev. Lett.* **101**, 131302 (2008).

[56] van den Hoogen, R. J., in *Proceedings of the Twelfth Marcel Grossmann Meeting on General Relativity, Eds. Damour, T., Jantzen, R. T. & Ruffini, R.*, World Scientific, Singapore (2011) [arXiv:1003.4020].

[57] Räsänen, S., *JCAP* **02**, 003 (2004).

[58] Barausse, E., Matarrese, S., & Riotto, A., *Phys. Rev. D* **71**, 063537 (2005).

[59] Gunn, J. E. & Gott, J. R., III, *Astrophys. J.* **176**, 1 (1972).

[60] Padmanabhan, T., *Structure Formation in the Universe*, Cambridge, UK (1993).

[61] Fosalba, P. & Gaztañaga, E., *Mon. Not. Roy. Astron. Soc.* **301**, 503 (1998).

[62] Abramo, L. R. *et al.*, *Phys. Rev. D* **79**, 023516 (2009).

[63] Stephani, H. *et al.*, *Exact Solutions of Einstein's Field Equations, Second Edition*, Cambridge University Press (2003).

[64] Célérier, M-N., *Astron. Astrophys.* **353**, 63 (2000).

[65] Moss, A., Zibin, J. P., & Scott, D., *Phys. Rev.* **D83**, 103515 (2011).

[66] Bolejko, K., Célérier, M-N., & Krasiǹski, A., *Class. Quant. Grav.* **28**, 164002 (2011).

[67] Célérier, M-N., Bolejko, K., & Krasiński, A., *Astron. Astrophys.* **518** A21 (2010).

[68] Biswas, T., Notari, A., & Valkenburg, W., *JCAP* **11**, 030 (2010).

[69] Nadathur, S. & Sarkar, S., *Phys. Rev.* **D83**, 063506 (2011).

[70] Bolejko, K., Hellaby, C., & Alfedeel, A. H. A., *JCAP* **09**, 011 (2011).

[71] Bolejko, K. & Andersson, L., *JCAP* **10**, 003 (2008).

[72] Paranjape, A. & Singh, T. P., *Class. Quant. Grav.* **23**, 6955 (2006).

[73] Räsänen, S., *JCAP* **11**, 010 (2004).

[74] Sussman, R. A., *Class. Quant. Grav.* **28** 235002 (2011).

[75] Alnes, H. & Amarzguioui, M., *Phys. Rev. D* **74**, 103520 (2006).

[76] García-Bellido, J. & Haugbølle, T., *JCAP* **09**, 016 (2008).

[77] Bull, P., Clifton, T., & Ferreira, P. G., *Phys. Rev. D* **85**, 024002 (2012).
[78] Zibin, J. P., *Phys. Rev. D* **84**, 123508 (2011).
[79] Romano, A. E., *JCAP* **05**, 020 (2010).
[80] García-Bellido, J. & Haugbølle, T., *JCAP* **04**, 003 (2008).
[81] Bolejko, K. & Wyithe, J., *JCAP* **02**, 020 (2009).
[82] Célérier, M-N., Bolejko, K., & Krasiǹski, A., *Astron. Astrophys.* **518**, A21 (2010).
[83] Biswas, T., Notari, A., & Valkenburg, W., *JCAP* **1011**, 030 (2010).
[84] Yoo, C-M., Nakao, K., & Sasaki, M., *JCAP* **07**, 012 (2010).
[85] Nadathur, S. & Sarkar, S., *Phys. Rev. D* **83**, 063506 (2011).
[86] Chuang, C-H., Gu, J-A., & Hwang, W-Y. P., *Class. Quant. Grav.* **25**, 175001 (2008).
[87] Kai, T. *et al.*, *Prog. Theor. Phys.* **117**, 229 (2007).
[88] Romano, A. E., *Phys. Rev. D* **75**, 043509 (2007).
[89] Räsänen, S., *JCAP* **02**, 011 (2009).
[90] Räsänen, S., *JCAP* **03**, 018, (2010).
[91] Bolejko, K. & Ferreira, P. G., (2012) [arXiv:1204.0909].
[92] Sinclair, B., Davis, T. M., & Haugbølle, T., *Astrophys. J.* **718**, 1445 (2010).